Magneto-Josephson effects in junctions with Majorana bound states

Liang Jiang, David Pekker, Jason Alicea, Gil Refael, Yuval Oreg, Arne Brataas, and Felix von Oppen

Phys. Rev. B **87**, 075438 — Published 25 February 2013

DOI: 10.1103/PhysRevB.87.075438

Magneto-Josephson effects in junctions with Majorana bound states

Liang Jiang[1,2], David Pekker[1], Jason Alicea[1,3], Gil Refael[1,6], Yuval Oreg[4], Arne Brataas[5], and Felix von Oppen[6]
[1] *Department of Physics, California Institute of Technology, Pasadena, California 91125, USA*
[2] *Department of Applied Physics, Yale University, New Haven, Connecticut 06511, USA*
[3] *Department of Physics and Astronomy, University of California, Irvine, California 92697, USA*
[4] *Department of Condensed Matter Physics, Weizmann Institute of Science, Rehovot, 76100, Israel*
[5] *Department of Physics, Norwegian University of Science and Technology, N-7491 Trondheim, Norway and*
[6] *Dahlem Center for Complex Quantum Systems and Fachbereich Physik, Freie Universität Berlin, 14195 Berlin, Germany*

We investigate 1D quantum systems that support Majorana bound states at interfaces between topologically distinct regions. In particular, we show that there exists a duality between particle-hole and spin degrees of freedom in certain spin-orbit-coupled 1D platforms such as topological insulator edges. This duality results in a spin analogue of previously explored 'fractional Josephson effects'—that is, the *spin current* flowing across a magnetic junction exhibits 4π periodicity in the relative magnetic field angle across the junction. Furthermore, the interplay between the particle-hole and spin degrees of freedom results in unconventional magneto-Josephson effects, such that the Josephson *charge current* is a function of the magnetic field orientation with periodicity 4π.

I. INTRODUCTION

The possibility of observing Majorana zero-modes in condensed matter has captured a great deal of attention in recent years. Much effort in this pursuit presently focuses on spin-orbit-coupled 1D wires, which are closely related to edges of 2D topological insulators (TIs). In either setting Majorana modes are predicted to localize through the competition between superconducting proximity effects and Zeeman splitting [1–7]. Remarkably, zero-bias conductance anomalies [8–12] possibly originating from Majorana modes have been observed very recently in quantum wires [13–15]. Numerous other fascinating phenomena tied to Majorana fermions have also been explored, including non-Abelian statistics [16–18], electron teleporation [19], and exotic Josephson effects [1, 4, 20].

Particularly interesting to us here are the Majorana-related Josephson effects in quantum wires and TI edges. Consider two Majorana modes hybridized across a Josephson junction formed by topological superconducting regions separated by a narrow barrier as shown in Fig. 1(b). The energy splitting of these Majoranas depends periodically on *half* the phase difference between the right and left superconductors, $(\phi_r - \phi_l)/2$, giving rise to a Josephson current with 4π periodicity in $\phi_r - \phi_l$ [1, 20]. If, in addition, a third superconductor contacts the middle domain, a difference between its phase and the *average* phase $(\phi_r + \phi_l)/2$ induces a non-local three-leg "zipper" Josephson current that divides equally between the two leads and is also 4π periodic in ϕ_r and ϕ_l [4]. These 'fractional Josephson effects' provide smoking-gun signatures of Majorana modes.

Our claim is that physical quantities of Majorana junctions in wires and TI edges can also possess 4π-periodic dependence on the *orientations* of Zeeman fields applied in the plane normal to the spin orbit direction. Notably, in some domain configurations the Majorana-mediated Josephson current *reverses sign* after a full 2π rotation of the magnetic field orientation on one side of the junction. An additional 2π rotation restores the current to its original direction. Thus the mixing between the particle-hole and spin degrees of freedom leads to an *unconventional magneto-Josephson effect* mediated through the coupled Majoranas.

Additionally, 'spin Josephson current' [21–24] may flow across the magnets providing the Zeeman energy, and also be 4π periodic in the field orientations as a manifestation of the Majorana modes. Define θ_s as the angle between the wire and the Zeeman field at domain s. Spin Josephson currents, j^S, are equivalent to torques [25] (driven partly by the Majoranas) that the wire domains apply on the external magnets [38]. Therefore, they are given by the derivative of the system's energy with respect to the magnetic field orientations θ:

$$j^S = \frac{\partial \langle \mathcal{H} \rangle}{\partial \theta}. \tag{1}$$

with $\mathcal{H}$ being the system's Hamiltonian. In the case of TI edges, the spin currents arise as the exact duals of Josephson currents, and the orientation of the B-field is the exact dual to the superconducting phase (indeed, the Josephson current is given by $j^Q = \frac{2e}{\hbar}\frac{\partial \langle \mathcal{H} \rangle}{\partial \phi}$)[39]. We emphasize that the 4π periodicity prevails as long as the parity of the Majorana state remains constant during the measurement, or changes at a slower rate than the winding of the superconducting phase and magnetic orientations.

This paper is organized as follows. In Sec. II, we consider the TI edges, calculate the Majorana coupling energy, discuss the Majorana-Josephson and spin Josephson effects, and discuss the duality between particle-hole and spin degrees of freedom. Then, we consider the corresponding effects in semiconductor quantum wire systems in Sec. III. Finally, in Sec. IV we propose several experimental implementations to observe these unconventional Josephson effects related to Majoranas, before we present our conclusion in Sec. V.

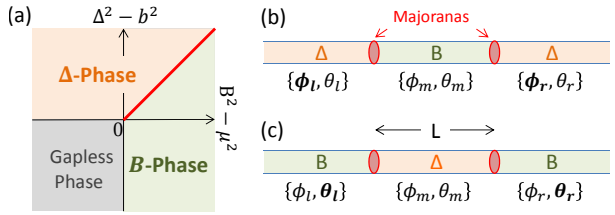

FIG. 1: (color online). (a) Phase diagram for 1D system: gapless-phase ($B^2 \leq \mu^2$ and $\Delta^2 \leq b^2$), Δ-phase ($\Delta^2 - b^2 > \max\left[B^2 - \mu^2, 0\right]$), and B-phase ($B^2 - \mu^2 > \max\left[\Delta^2 - b^2, 0\right]$). Both Δ-phase and B-phase are gapped. (b) The Δ-B-Δ junction supports Majorana bound states at the domain walls [4]. (c) The dual configuration of B-Δ-B junction that also supports Majorana bound states at the domain walls.

II. MAJORANAS ON TI EDGES

Let us focus first on the analysis of the 4π-periodic orientation dependence in TI edges, before commenting on spin-orbit-coupled wires which obey qualitatively similar rules. The Hamiltonian, including s-wave pairing and Zeeman fields in both the transverse and parallel directions relative to the spin-orbit direction, reads

$$\mathcal{H} = v\hat{p}\tau^z\sigma^z - \mu\tau^z + \Delta\left(\cos\phi\ \tau^x - \sin\phi\ \tau^y\right) - b\sigma^z + B\left(\cos\theta\ \sigma^x - \sin\theta\ \sigma^y\right). \quad (2)$$

Here we have employed the Nambu spinor basis $\Psi^T = (\psi_\uparrow, \psi_\downarrow, \psi_\downarrow^\dagger, -\psi_\uparrow^\dagger)$ and introduced Pauli matrices σ^a and τ^a that act in the spin and particle-hole sectors, respectively. The edge-state velocity is given by v, $\hat{p}$ is the momentum, and the σ^z-direction represents the spin-orbit-coupling axis. We allow the chemical potential μ, superconducting pairing $\Delta e^{i\phi}$, longitudinal magnetic field strength b, transverse magnetic field strength B, and the transverse-field orientation angle θ to vary spatially. Interestingly, Eq. (2) has a *magnetism-superconductivity duality*—the Hamiltonian takes the same form upon interchanging the magnetic terms $\{b, B, \theta, \sigma^a\}$ with the superconducting terms $\{\mu, \Delta, \phi, \tau^a\}$, which was first pointed out in the footnote of Ref. [37]. This duality sheds light on various unconventional physical consequences.

The Hamiltonian (2) supports three different phases determined by the relative strength of $\{\Delta, \mu, B, b\}$. As Fig. 1(a) illustrates, we have (i) a topological superconducting gapped phase (denoted henceforth as the Δ-phase) when $\Delta^2 - b^2 > \max\left[B^2 - \mu^2, 0\right]$, (ii) a topological magnetic gapped phase (denoted B-phase) when $B^2 - \mu^2 > \max\left[\Delta^2 - b^2, 0\right]$, and (iii) a trivial gapless state when $B^2 \leq \mu^2$ and $\Delta^2 \leq b^2$ (see detailed discussion in Appendix A). Consistent with the magnetic-superconducting duality, in the phase diagram of Fig. 1(a) the B- and Δ-phases are symmetrically arranged with respect to the diagonal line that defines the boundary between these two gapped states:

$$\Delta^2 + \mu^2 = B^2 + b^2. \quad (3)$$

One Majorana zero-mode binds to each domain wall separating B- and Δ-domains. For notational simplicity, below we will assume that $\Delta > b > 0$ and $B > \mu > 0$, though more general results can be obtained (see Appendix C). We will also focus on setups for which all domains experience both superconductivity and a transverse Zeeman field.

A. Majorana Coupling

In TI edges, the 4π periodic dependence on the magnetic field orientation occurs when two Majoranas are nestled in a B-Δ-B domain sequence as in Fig. 1(c). This is in contrast to the previously studied unconventional Josephson effects [1, 4, 20], which occur over a junction between two Δ-domains bridged by a B-domain [see Fig. 1(b)]. The magneto-Josephson and spin-Josephson effects of a TI edge follow from the detailed dependence of the Majorana energy splitting, $E_{\rm Maj}$, on the field orientations and superconducting phases in the B-Δ-B edge domain structure of Fig. 1(c). In addition to an exact numerical calculation of $E_{\rm Maj}$, we provide in Appendix B an analytical variational approach that sheds light on the physics. In the latter approach we assume that the two Majorana wavefunctions ($|L\rangle$ and $|R\rangle$) are unmodified by their proximity to each other, apart from being superposed to form a conventional low-lying state. This leads to an energy splitting that is suppressed as a weighted sum of two exponentials which control the decay of the Majorana wave functions in the middle domain.

Our results for the Majorana couplings constitute one of the central results of this paper. The *two* characteristic decay lengths as a function of field and pairing are $\lambda_{1,2} = \frac{v}{|\sqrt{\Delta^2 - b^2} \pm \sqrt{B^2 - \mu^2}|}$, which characterizes the localized Majorana wavefunctions. When the overlap of the wavefunction is small $|\langle L|R\rangle| \ll \sqrt{\langle L|L\rangle \langle R|R\rangle}$, the coupling energy between $|L\rangle$ and $|R\rangle$ is approximately $E_{\rm Maj} \approx \frac{\langle L|H|R\rangle}{\sqrt{\langle L|L\rangle \langle R|R\rangle}}$, which can be computed from the explicit form of the wavefunctions of $|L\rangle$ and $|R\rangle$ (see Appendix B). Quite generally, for the middle Δ-domain of length L, the Majorana coupling energy is:

$$\frac{E_{\rm Maj}}{E_0\left[\delta\phi_{l,r}\right]} \approx e^{-\lambda_{m,1}L} \sin\frac{\delta\theta_l - \tilde{\mu}_m + \tilde{\mu}_l}{2} \sin\frac{\delta\theta_r + \tilde{\mu}_m - \tilde{\mu}_r}{2} - e^{-\lambda_{m,2}L} \sin\frac{\delta\theta_l + \tilde{\mu}_m + \tilde{\mu}_l}{2} \sin\frac{\delta\theta_r - \tilde{\mu}_m - \tilde{\mu}_r}{2}, \quad (4)$$

with $\delta\phi_{\ell,r} \equiv \phi_{\ell,r} - \phi_m$, $\delta\theta_{\ell,r} \equiv \theta_{\ell,r} - \theta_m$, $\tilde{\mu}_{l/m/r} \equiv \cos^{-1}\frac{\mu_{l/m/r}}{B_{l/m/r}}$, $\tilde{b}_{l/m/r} \equiv \cos^{-1}\frac{b_{l/m/r}}{\Delta_{l/m/r}}$, and the characteristic energy

$$E_0\left[\delta\phi_{l,r}\right] = \frac{\sin\tilde{b}_m}{\sin\tilde{\mu}_m}\frac{1}{\sqrt{M_l\left[\delta\phi_l\right]M_r\left[\delta\phi_r\right]}}. \tag{5}$$

The denominator of E_0 follows from

$$M_s\left[\delta\phi_s\right] \approx \frac{\left(\Delta_m^2+\mu_m^2-b_m^2\right)}{2\sqrt{\Delta_m^2-b_m^2}\left(\Delta_m^2+\mu_m^2-B_m^2-b_m^2\right)} + \frac{\left(B_s^2+b_s^2-\mu_s^2\right)+\Delta_s\left[\sqrt{B_s^2-\mu_s^2}\sin\left(\tilde{b}_m\pm\delta\phi_s\right)-b_s\cos\left(\tilde{b}_m\pm\delta\phi_s\right)\right]}{2\sqrt{B_s^2-\mu_s^2}\left(B_s^2+b_s^2-\Delta_s^2-\mu_s^2\right)}, \tag{6}$$

with the choice of sign $\pm$ depending on $s = l$ or r. Note that M_s exhibits the standard 2π periodicity in ϕ_s, so that the more exotic 4π periodicity follows exclusively from the trigonometric functions in Eq. (4).

B. Magneto-Josephson Effects

These general results allow us to quantitatively estimate the magneto-Josephson effects described earlier, which can be measured in the circuit sketched in Fig. 2(a). For simplicity, we specialize to the case of $\mu_{l/m/r} = 0$, where the Majorana coupling energy reduces to

$$E_{\rm Maj} \approx \epsilon_M[\delta\phi_{\ell,r}]\cos\frac{\theta_l-\theta_r}{2} + \epsilon_Z[\delta\phi_{\ell,r}]\cos\frac{\theta_l+\theta_r-2\theta_m}{2}, \tag{7}$$

with $\epsilon_{M/Z}[\delta\phi_{\ell,r}] = E_0[\delta\phi_{\ell,r}]\left(e^{-L/\lambda_{m,2}} \pm e^{-L/\lambda_{m,1}}\right)/2$.

The Majorana-related magneto-Josephson currents entering the $s = \ell/r$ electrode are $j_s^Q = \frac{2e}{\hbar}\frac{\partial\langle\mathcal{H}\rangle}{\partial\phi_s} = p\frac{2e}{\hbar}\frac{E_{\rm Maj}}{\partial\phi_s}$, where $p = \pm1$ denotes the parity of the hybridized Majoranas. The explicit form for the charge currents (dropping the parity factor p) is:

$$j_{\ell/r}^Q \approx \pm j_M^Q\cos\tfrac{\theta_l-\theta_r}{2} + j_Z^Q\cos\tfrac{\theta_l+\theta_r-2\theta_m}{2}, \quad \text{with: } j_{M/Z}^Q = \tfrac{2e}{\hbar}\tfrac{\partial\epsilon_{M/Z}}{\partial\phi_{\ell/r}}. \tag{8}$$

which constitutes a prediction for the unconventional magneto-Josephson effect. The analytical expressions obtained above for j_M^Q and j_Z^Q agree well with the numerical calculations for large L as shown in Fig. 2(b). They confirm that for B-Δ-B junctions the Majorana coupling induces the charge current $j_{l/r}^Q$ with 4π periodic dependence on $\theta_{l/r}$.

C. Spin Josephson Effects

Similarly the spin Josephson currents, or torques on the magnets, in region $s = \ell/r$ are $j_s^S = -\frac{\partial\langle\mathcal{H}\rangle}{\partial\theta_s} = p\frac{\partial E_{\rm Maj}}{\partial\theta_s}$ [Eq. (1)]. The angular momentum transferred by these currents is in the direction parallel to the spin-orbit axis, which in this case is the z-direction. The spin Josephson currents are thus given by:

$$j_{l/r}^S = \pm j_M^S\sin\tfrac{\theta_l-\theta_r}{2} + j_Z^S\sin\tfrac{\theta_l+\theta_r-2\theta_m}{2}, \quad \text{with: } j_{M/Z}^S = \tfrac{\epsilon_{M/Z}}{2}. \tag{9}$$

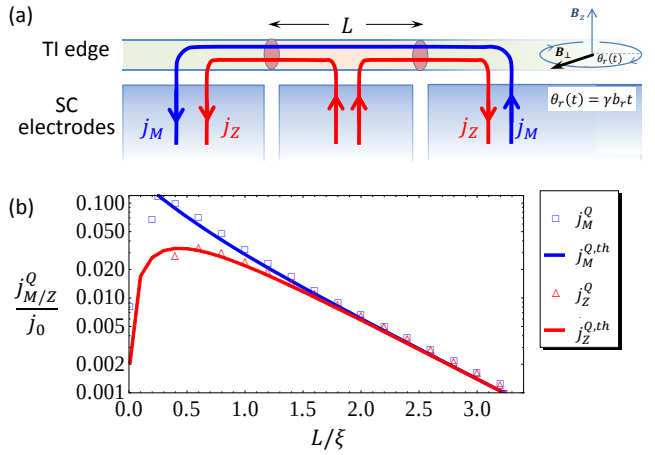

FIG. 2: (color online). (a) The scheme to measure unconventional magneto-Josephson effect. Josephson currents are measured for the B-Δ-B junction. In the right region, the transverse magnetic field winds at rate $\omega_L = \gamma b_r$, which modulates the Josephson current at *half* the frequency, $\omega_L/2$. (b) Comparison between analytical expressions and numerical results for j_M and j_Z. The parameters are $\mu_{l/m/r} = 0$, $b_{l/m/r} = E/2$, $\Delta_m = 2.5E$, $\Delta_{l/r} = E$, $B_{l/r} = 2E$, $B_m = E$. For $E = 0.1$meV and $v = 10^4$m/s, the length unit is $\xi = 66$nm and the current unit is $j_0 = 50$nA. The superconducting angles are fixed $\phi_{l/r} = \pi/2$, $\phi_m = 0$.

The j_M^S spin current exchanges angular momentum between the right and left magnets directly, while the j_Z^S spin current originates in the middle region and equally splits into the right and left regions, $j_{m\to l}^S = j_{m\to r}^S = j_Z^S\sin\frac{\theta_l+\theta_r-2\theta_m}{2}$. This term vanishes when there is no transverse magnetic field in the middle domain, and represents the dual of the zipper Josephson effect in the Δ-B-Δ junction that splits charge current from the middle domain between the two side domains [4].

D. Duality

The origin of this exotic dependence of the Majorana-related currents can be traced to the magnetic-

superconducting duality in topological insulator edges [1, 4]. For a junction with three alternating domains, there are two dual configurations: the Δ-B-Δ junction [Fig. 1(b)] and the B-Δ-B junction [Fig. 1(c)]. The spin-Josephson effect in the B-Δ-B junction is dual to the charge-Josephson effect in the Δ-B-Δ junction [1–4]. Similarly, the magneto-Josephson effect depending on the orientation angles in the B-Δ-B junction has a dual spin-Josephson effect depending on the superconducting angles in the Δ-B-Δ junction.

III. QUANTUM WIRE

Majorana junctions in spin-orbit coupled semiconductor wires exhibit the same magneto-Josephson and spin-Josephson effects as the TI edge. The principle difference is that for a wire there is a kinetic energy term $\mathcal{H}_k = \frac{1}{2m}\hat{p}^2\tau^z$ added to Eq. (2), which produces additional Fermi points at 'large' momenta $p_F \sim \pm 2mv$. The wire's Hamiltonian supports a topological (T) phase and a non-topological (NT) phase that adiabatically connects to the vacuum [2, 3]. Because of the additional Fermi points, the semiconductor wire has 4π-periodic effects in both θ and ϕ for T-NT-T junctions, while it only has the trivial 2π-periodicity for NT-T-NT junctions [40]. The quantitative analysis of the magneto-, spin-, and charge-Josephson effects in wires as well as the role of Andreev bound states will be analyzed elsewhere [26].

IV. EXPERIMENTAL IMPLEMENTATION

Observing the unconventional magneto-Josephson effect and the 4π periodicity in $\theta_{l/r}$ [see Fig. 3(b)] requires effective control of the magnetic field orientation. In particular, the orientation change needs to be sufficiently fast so that the Majorana states' total parity does not change by relaxation processes [1, 20, 27], but still slow on the scale of the inverse bulk gap to avoid quasiparticle poisoning [28]. The rate of parity decay is strongly detail dependent, but we surmise that measurements with rates faster than 1 kHz and slower than the minimum gap in the device would suffice. Conventional magnets may be too unwieldy when made to rapidly turn; nuclear magnetization, however, could be ideal for this task. Through the hyperfine coupling, a polarized nuclear spin population could create an effective Zeeman field in the plane perpendicular to the spin-orbit coupling direction. For example, large nuclear spin polarization, normal to the spin-orbit direction, can be induced by optical pumping with circularly polarized light. The induced hyperfine transverse field can be rather strong, e.g., $B \sim 0.1$ Tesla for 2% nuclear polarization fraction in GaAs samples [29]. This process can exist in various materials, as long as optical pumping introduces nonequilibrium electron spins, which preferentially flip nuclear spins and induce nuclear hyperpolarization via the Overhauser effect [30]. In addition, an external magnetic field with strength b, applied parallel to the spin-orbit axis, will make the orientation angle of the hyperfine transverse field wind at a rate $\omega_L = \gamma b$, where $\gamma/2\pi \approx -7.6$ MHz/T for ^{199}Hg or $\gamma/2\pi \approx 13.5$ MHz/T for ^{125}Te nuclei [31]. Moreover, the nuclear polarization can persist for long times, limited by the inhomogeneous nuclear transverse spin lifetime $T_2^* \sim 100$ μs, which already suffices for hundreds of precession periods for $b \sim 0.1$ Tesla. The transverse spin lifetime can be further extended using spin echo techniques.

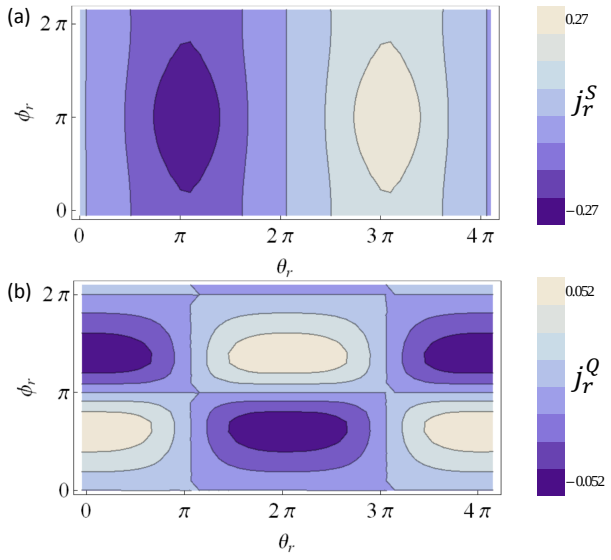

FIG. 3: (color online). Contour plot of (a) spin current j_r^S and (b) charge current j_r^Q, both of which are 4π periodic in θ_r and 2π periodic in ϕ_r. The other angles are fixed $\phi_l = \pi/2$, $\phi_m = \theta_{l/m} = 0$. The parameters are the same as Fig. 2.

With a rotating transverse magnetic field, we can observe the magneto-Josephson effect in several ways. A constantly winding orientation in the left domain, $\theta_r(t) = \omega_L t$ [while fixing $\theta_{l/m}(t) = 0$, as illustrated in Fig. 2(a)], produces an oscillatory component of the charge current with amplitude $j^Q_{\omega_L/2} = j^Q_M + j^Q_Z = \frac{2e}{\hbar}\frac{\partial E_0}{\partial \phi} e^{-L/\lambda_{m-}}$ at *half* the frequency, $\omega_L/2$. In TI edges, we can also use resonant properties to probe the orientation-frequency halving. A DC voltage V applied to the right superconducting lead, for instance, induces a winding of the superconducting angles, $\phi_r(t) = 2eVt/\hbar$ and $\phi_{l/m}(t) = 0$. When the magnetic orientation also winds with angular velocity Ω_L, interference between the two oscillation would yield a DC current from the right superconducting lead, when $\omega_L = 2\Omega_V$ (neglecting high-order resonances). The amplitude of the dc current is expected to be:

$$j^{Q,DC}_{\omega_L=2\Omega_V} \approx \frac{1}{2\pi}\int_0^{2\pi} j^Q_{\omega_L/2}[\phi_r]\cos\phi_r d\phi_r. \qquad (10)$$

Alternatively, one can apply an AC voltage to the right superconducting lead such that $\phi_r \propto \sin\omega t$, while all

other superconducting angles are held fixed. Interference effects now produce Shapiro-step-like resonant features which emerge only when

$$\omega_L = 2n\omega \tag{11}$$

for even integer $2n$ (neglecting higher order corrections to the θ dependence).

The Majorana-mediated spin currents with 4π phase periodicity are harder to measure. A possible route for such measurements is to use a magnetic nanoparticle as the magnetic field source on one of the side domains. The torques on the nanoparticle could be probed from the shift in the ferromagnetic resonance (FMR) frequency. The FMR frequency is typically $f_0 \sim 10$ GHz. The FMR linewidth, dictated by the Gilbert damping coefficient α, is of order $\alpha f_0 = 0.01 f_0$ in bulk ferromagnets, but is probably much smaller in nanoparticles [32]. A rough estimate of the maximum Majorana-related spin-current (or torque), j^S, yields $j^S \sim \hbar \cdot 10$ GHz. This produces a frequency shift around j^S/m_{total}, which is inversely proportional to the total angular momentum of the FM grain m_{total} [33]. This shift must dominate the FMR linewidth, $j^S/m_{total} > f_0\alpha$. The nanograin must, therefore, be sufficiently small such that $m_{total}/\hbar < \alpha^{-1} \sim 100$, e.g. have a radius of around 10 nm, and still provide a sufficient Zeeman field for the domain it is on.

Measuring the effect of the relative field orientation on the spin and charge currents can be complicated by the presence of conventional Josephson effects arising from the continuum states. Indeed, the bulk energy associated with the continuum states also has dependence on magnetic field orientations and superconducting phases that are interesting in their own right, and of similar magnitude to the Majorana related effects. Nonetheless, all these dependencies are 2π periodic, as we have confirmed numerically. Hence, the measurement schemes proposed above will be insensitive to them.

V. CONCLUSION

In conclusion, we explored consequences of a magnetism-superconductivity duality of TI edge states, emphasizing Josephson effects. Most prominently, the duality implies that spin and charge Josephson currents in TI edges exhibit a 4π periodic dependence on the orientation difference of the magnetic field. These remarkable effects are a direct consequence of the Majorana states and we make several proposals how to detect them experimentally. The duality is only approximate in spin-orbit-coupled quantum wires but analogous effects also occur in this system. In addition to the Josephson effects, the duality has further interesting implications. For instance, it implies that the transition between topological and trivial phases can be tuned using a magnetic gradient, which is the dual of the superconducting phase gradient [34].

Note added: As we were completing the manuscript we became aware of two overlapping works [35, 36].

Acknowledgment

It is a pleasure to thank M. P. A. Fisher, L. Glazman, A. Haim, B. Halperin, A. Kitaev, L. Kouwenhoven, C. Marcus, J. Meyer, Y. Most, F. Pientka, J. Preskill, X.L. Qi, K. Shtengel, and A. Stern for useful discussions, and the Aspen Center for Physics for hospitality. We are also grateful for support from the NSF through grant DMR-1055522, BSF, SPP1285 (DFG), NBRPC (973 program) grant 2011CBA00300 (2011CBA00301), the Alfred P. Sloan Foundation, the Packard Foundation, the Humboldt Foundation, the Minerva Foundation, the Sherman Fairchild Foundation, the Lee A. DuBridge Foundation, the Moore-Foundation funded CEQS, and the Institute for Quantum Information and Matter (IQIM) an NSF Physics Frontiers Center with support of the Gordon and Betty Moore Foundation.

Appendix A: Phase Diagram

In this Appendix, we characterize three different phases associated with the 1D quantum system characterized by the following Hamiltonian:

$$\begin{aligned} H(\mu,\Delta,\phi;b,B,\theta) = {} & p\tau^z\sigma^z - \mu\tau^z + \Delta\left(\tau^x\cos\phi - \tau^y\sin\phi\right) \\ & - b\sigma^z + B\left(\sigma^x\cos\theta - \sigma^y\sin\theta\right). \end{aligned} \tag{A1}$$

The six control parameters above include the chemical potential μ, pairing energy Δ, superconducting phase ϕ, longitudinal magnetic field $-b$, and transverse field B with orientation angle θ. In this form, the duality between (Δ,μ) and (B,b) is more obvious. Without loss of generality, we assume that all the control parameters (μ,Δ,b,B) are all positive. We compute the determinant

$$\begin{aligned} \det H = {} & \left[p^2 + \left(\sqrt{B^2-\mu^2} + \sqrt{\Delta^2-b^2}\right)^2\right] \\ & \left[p^2 + \left(\sqrt{B^2-\mu^2} - \sqrt{\Delta^2-b^2}\right)^2\right]. \end{aligned} \tag{A2}$$

The energy gap is closed if there exist real solutions of p to satisfy $\det H = 0$.

1. When $B^2 \le \mu^2$ and $\Delta^2 \le b^2$, the system is in a **gapless-phase**, because there are real solutions $p = \pm\left(\sqrt{-B^2+\mu^2} + \sqrt{-\Delta^2+b^2}\right)$ or $p = \pm\left(\sqrt{-B^2+\mu^2} - \sqrt{-\Delta^2+b^2}\right)$ to fulfill the requirement of $\det H = 0$.

2. When $B^2 > \mu^2$ or $\Delta^2 > b^2$, the system is always gapped, because there are no real solutions of p to satisfy $\det H = 0$.

   (a) For $\Delta^2 - b^2 > \max\left[B^2-\mu^2, 0\right]$, the system is in a superconducting gapped phase (**Δ-phase**).

(b) For $B^2-\mu^2 > \max\left[\Delta^2-b^2, 0\right]$, the system is in a magnetic gapped phase (B**-phase**).

(c) There is a quantum phase transition at $\Delta^2 - b^2 = B^2-\mu^2$, which connects the Δ-phase and the B-phase.

Therefore, we obtain the phase diagram in Fig. 1(a) of the maintext.

Appendix B: Majorana Coupling

Here we consider the B-Δ-B junction and calculate the Majorana coupling.

1. 1D System Consisting of Different Regions

We are interested in the case that the 1D system consists of three regions of different control parameters. Specifically

$$\chi = \begin{cases} \chi_l & \text{for } x \in (-\infty, 0) \\ \chi_m & \text{for } x \in (0, L) \\ \chi_r & \text{for } x \in (L, +\infty) \end{cases} \tag{B1}$$

with χ representing the six control parameters. The system Hamiltonian is

$$H = \begin{cases} H_l & \text{for } x \in (-\infty, 0) \\ H_m & \text{for } x \in (0, L) \\ H_r & \text{for } x \in (L, +\infty) \end{cases} \tag{B2}$$

with $H_f \equiv H\left(\mu_f, \Delta_f, \phi_f; b_f, B_f, \theta_f\right)$. We are interested in the B-Δ-B configuration, with $B_l^2 - \mu_l^2 > \max\left[\Delta_l^2 - b_l^2, 0\right]$, $\Delta_m^2 - b_m^2 > \max\left[B_m^2 - \mu_m^2, 0\right]$, and $B_r^2 - \mu_r^2 > \max\left[\Delta_r^2 - b_r^2, 0\right]$.

2. Perturbative Calculation of the Coupling Energy

Let's first consider the individual Majoranas. The left Majorana $|L\rangle$ is at $x = 0$ associated with the $l-m$ boundary. We may introduce the Hamiltonian $H_L = \begin{cases} H_l & \text{for } x \in (-\infty, 0) \\ H_m & \text{for } x \in (0, \infty) \end{cases}$ that supports the zero energy Majorana mode $|L\rangle$, with $H_L|L\rangle = 0$. Similarly, the right Majorana $|R\rangle$ is at $x = L$ associated with the $m-r$ boundary. We can also introduce $H_R = \begin{cases} H_m & \text{for } x \in (-\infty, L) \\ H_r & \text{for } x \in (L, +\infty) \end{cases}$ that supports zero-energy Majorana mode $|R\rangle$, with $H_R|R\rangle = 0$. We can can perturbatively compute the coupling energy between $|L\rangle$ and $|R\rangle$ by the formula:

$$\mathcal{H}_{LR} \approx M^{-1/2} h M^{-1/2} \tag{B3}$$

with $M = \begin{pmatrix} \langle L|L\rangle & \langle L|R\rangle \\ \langle R|L\rangle & \langle R|R\rangle \end{pmatrix}$ being the overlap matrix between the (not necessarily normalized) Majorana states, and h being:

$$h = \begin{pmatrix} 0 & \langle L|\,\Delta V\,|R\rangle \\ \langle R|\,\Delta V\,|L\rangle & 0 \end{pmatrix} \tag{B4}$$

with:

$$\Delta V = H - H_L = (H_r - H_m)\,\eta\,(x - L)\,, \tag{B5}$$

where η is the Heaviside step function. For separated Majorana modes, the overlap of the wavefunction is small $|\langle L|R\rangle| \ll \sqrt{\langle L|L\rangle\langle R|R\rangle}$. Therefore, the coupling Hamiltonian is approximately $\mathcal{H}_{LR} \approx \begin{pmatrix} 0 & E \\ E^* & 0 \end{pmatrix}$, with

$$E \approx \frac{\langle L|\,\Delta V_L\,|R\rangle}{\sqrt{\langle L|L\rangle\langle R|R\rangle}}. \tag{B6}$$

3. Wavefunction of Individual Majoranas

We can rewrite the Hamiltonian as

$$H_L = H_l\eta(-x) + H_m\eta(x) \tag{B7}$$

$$= \begin{cases} U_l \cdot V \cdot (p - K_l) \cdot V^\dagger \cdot U_l^\dagger \tau^z\sigma^z & \text{for } x < 0 \\ U_m \cdot V \cdot (p - K_m) \cdot V^\dagger \cdot U_m^\dagger \tau^z\sigma^z & \text{for } x > 0 \end{cases}. \tag{B8}$$

where the unitary transformations are

$$V = e^{-i\frac{\pi}{4}\tau^z\sigma^z} \tag{B9}$$

$$U = e^{i\frac{\phi}{2}\tau^z} \otimes e^{i\frac{\theta}{2}\sigma^z} \equiv: U_\phi \otimes U_\theta \tag{B10}$$

and the non-Hermitian matrix is

$$K = (b\tau^z + i\Delta\tau^x) + (\mu\sigma^z + iB\sigma^x) \tag{B11}$$

with sub-index $f = l, m, r$ not explicitly written for simplicity. Without loss of generality, we can fix

$$\phi_m = \theta_m = 0 \tag{B12}$$

and $U_m = I$. For our notational convenience, we also introduce

$$\tilde{b} \equiv \cos^{-1}\frac{b}{\Delta} \tag{B13}$$

and

$$\tilde{\mu} \equiv \cos^{-1}\frac{\mu}{B}. \tag{B14}$$

Here we assume $\Delta^2 > b^2$ and $B^2 > \mu^2$ for simplicity. (We will relax this parameter constraint by analytic continuation.)

The eigensystem of K is

$$K\cdot\left(v_{\tilde{b}}^{s_1}\otimes v_{\tilde{\mu}}^{s_2}\right)=\Lambda^{s_1,s_2}\left(v_{\tilde{b}}^{s_1}\otimes v_{\tilde{\mu}}^{s_2}\right) \tag{B15}$$

with sub-eigenvectors

$$v_\xi^s=\frac{1}{\sqrt{2}}\left(-ie^{is\xi/2},e^{-is\xi/2}\right)^T=v_{s\xi}^+ \tag{B16}$$

and eigenvalues

$$\Lambda^{s_1,s_2}=\Delta\ \lambda_{\tilde{b}}^{s_1}+B\ \lambda_{\tilde{\mu}}^{s_2} \tag{B17}$$

where

$$\lambda_\xi^s=\lambda_{s\xi}^+=i\sin s\xi \tag{B18}$$

for $s=\pm1$. $\left(v_\xi^+\right)^T\cdot v_{\xi'}^+=-i\sin\frac{\xi+\xi'}{2}$. The two-vectors $v_\xi^s=v_{s\xi}^+$ have the following properties of inner-products:

$$\left(v_\xi^s\right)^T\cdot v_\xi^{s'}=-i\sin s\xi\ \delta_{s,s'}=\begin{pmatrix}-i\sin\xi & 0\\ 0 & i\sin\xi\end{pmatrix} \tag{B19}$$

$$\left(v_\xi^s\right)^\dagger\cdot\sigma^z\cdot v_\xi^{s'}=-i\sin s\xi\ \delta_{\bar{s},s'}=\begin{pmatrix}0 & -i\sin\xi\\ i\sin\xi & 0\end{pmatrix} \tag{B20}$$

$$\left(v_\xi^s\right)^\dagger\cdot v_\xi^{s'}=\delta_{s,s'}+\cos\xi\ \delta_{\bar{s},s'}=\begin{pmatrix}1 & \cos\xi\\ \cos\xi & 1\end{pmatrix} \tag{B21}$$

where $\bar{s}:\equiv -s$ for $s=\pm1$. And it transforms under the unitary

$$U_\theta v_\xi^+=v_{\theta+\xi}^+. \tag{B22}$$

a. ***Left Majorana.*** For the $B-\Delta$ interface at $x=0$, the localized zero-energy eigenstate is

$$|L\rangle=\begin{cases}V\cdot U_l\cdot\tau^z\sigma^z\left|\Psi_\alpha\right\rangle & \text{for } x<0\\ V\cdot U_m\cdot\tau^z\sigma^z\left|\Psi_\beta\right\rangle & \text{for } x>0\end{cases}, \tag{B23}$$

with

$$\Psi_\alpha(x)=\sum_s v_{\tilde{b}_l}^s\otimes v_{\tilde{\mu}_l}^+\ \alpha_s e^{-i\Lambda_l^{s,+}x} \tag{B24}$$

$$\Psi_\beta(x)=\sum_s v_{\tilde{b}_m}^-\otimes v_{\tilde{\mu}_m}^s\ \beta_s e^{-i\Lambda_m^{-,s}x}. \tag{B25}$$

One can verify

$$H_L\left|L\right\rangle=0 \tag{B26}$$

because

$$\begin{cases}(p-K_l)\left|\Psi_\alpha\right\rangle=0 & \text{for } x<0\\ (p-K_m)\left|\Psi_\beta\right\rangle=0 & \text{for } x>0\end{cases}. \tag{B27}$$

The boundary condition $|L(x=0^-)\rangle=|L(x=0^+)\rangle$ requires

$$U_l\left|\Psi_\alpha\left(x=0^-\right)\right\rangle=\left|\Psi_\beta\left(x=0^+\right)\right\rangle, \tag{B28}$$

and hence

$$\sum_s v_{s\tilde{b}_l}^+\ \alpha_s=U_{-\phi_l}v_{-\tilde{b}_m}^+ \tag{B29}$$

$$\sum_s v_{s\tilde{\mu}_m}^+\ \beta_s=U_{\theta_l}v_{\tilde{\mu}_l}^+ \tag{B30}$$

which gives us

$$\alpha_s=\sin^{-1}\left(s\tilde{b}_l\right)\sin\left(\frac{s\tilde{b}_l-\left(\phi_l+\tilde{b}_m\right)}{2}\right) \tag{B31}$$

$$\beta_s=\sin^{-1}\left(s\tilde{\mu}_m\right)\sin\left(\frac{s\tilde{\mu}_m+(\theta_l+\tilde{\mu}_l)}{2}\right). \tag{B32}$$

b. ***Right Majorana.*** Similarly, For the $\Delta-B$ interface at $x=L$, the localized zero-energy eigenstate is

$$|R\rangle=\begin{cases}V\cdot U_m\cdot\tau^z\sigma^z\left|\Psi_\gamma\right\rangle & \text{for } x<L\\ V\cdot U_r\cdot\tau^z\sigma^z\left|\Psi_\delta\right\rangle & \text{for } x>R\end{cases}, \tag{B33}$$

with

$$\Psi_\gamma(x)=\sum_s v_{\tilde{b}_m}^+\otimes v_{\tilde{\mu}_m}^s\ \gamma_s e^{-i\Lambda_m^{+,s}(x-L)} \tag{B34}$$

$$\Psi_\delta(x)=\sum_s v_{\tilde{b}_r}^s\otimes v_{\tilde{\mu}_r}^-\ \delta_s e^{-i\Lambda_r^{s,-}(x-L)}. \tag{B35}$$

and

$$\gamma_s=\sin^{-1}\left(s\tilde{\mu}_m\right)\sin\left(\frac{s\tilde{\mu}_m+(\theta_r-\tilde{\mu}_r)}{2}\right) \tag{B36}$$

$$\delta_s=\sin^{-1}\left(s\tilde{b}_l\right)\sin\left(\frac{s\tilde{b}_r-\left(\phi_r-\tilde{b}_m\right)}{2}\right). \tag{B37}$$

4. Normalization of Wavefunctions

The normalization of wavefunction is

$$\begin{aligned} M_l\left[\phi_l\right] \equiv \langle L|L\rangle &= \int_0^\infty dx \left\langle \Psi_\beta\left(x\right)\right| \left.\Psi_\beta\left(x\right)\right\rangle + \int_{-\infty}^0 dx \left\langle \Psi_\alpha\left(x\right)\right| \left.\Psi_\alpha\left(x\right)\right\rangle \\ &\approx \frac{\left(\Delta_m^2+\mu_m^2-b_m^2\right)}{2\sqrt{\Delta_m^2-b_m^2}\left(\Delta_m^2+\mu_m^2-B_m^2-b_m^2\right)} + \frac{\left(B_l^2+b_l^2-\mu_l^2\right)+\Delta_l\left[\sqrt{B_l^2-\mu_l^2}\sin\left(\tilde{b}_m+\phi_l\right)-b_l\cos\left(\tilde{b}_m+\phi_l\right)\right]}{2\sqrt{B_l^2-\mu_l^2}\left(B_l^2+b_l^2-\Delta_l^2-\mu_l^2\right)} \end{aligned} \tag{B38}$$

Note that the each of the two terms are positive definite, because $B_l^2+b_l^2>\Delta_l^2+\mu_l^2$ and $\Delta_m^2+\mu_m^2>B_m^2+b_m^2$. By taking $\mu_f=0$ (i.e., $\tilde{\mu}_f=\pi/2$), $b_{l,m,r}=0$ (i.e., $\tilde{b}_{l,m,r}=\pi/2$), we have the expressions

$$\langle L|L\rangle_{00} = \frac{\Delta_m}{2\left(\Delta_m^2-B_m^2\right)} + \frac{B_l+\Delta_l\cos\phi_l}{2\left(B_l^2-\Delta_l^2\right)}. \tag{B39}$$

We can also compute $M_r\left[\phi_r\right]\equiv\langle R|R\rangle$, which is very similar to $M_l\left[\phi_l\right]$ with the following replacement

$$\tilde{b}_m+\phi_l \Longrightarrow \tilde{b}_m-\phi_r \tag{B40}$$

$$\Delta_l,\mu_l,B_l,b_l \Longrightarrow \Delta_r,\mu_r,B_r,b_r \tag{B41}$$

5. Cross Coupling $\langle L|\,\Delta V_L\,|R\rangle$

We now compute the cross coupling term $\langle L|\,\Delta V_L\,|R\rangle$. First, we can rewrite ΔV_L

$$\Delta V_L = -U_r\cdot V\cdot\left(p-K_r\right)\cdot V^\dagger\cdot U_r^\dagger\tau^z\sigma^z\times\eta\left(x-L\right)+U_m\cdot V\cdot\left(p-K_m\right)\cdot V^\dagger\cdot U_m^\dagger\cdot\tau^z\sigma^z\times\eta\left(x-L\right). \tag{B42}$$

The matrix element can be calculated as

$$\begin{aligned} \langle L|\,\Delta V_L\,|R\rangle &= -\int_L^\infty dx \left\langle \Psi_\beta\left(x\right)\right| U_m^\dagger\cdot U_r\cdot\tau^z\sigma^z\cdot K_r\left|\Psi_\delta\left(x\right)\right\rangle + \int_L^\infty dx \left\langle \Psi_\beta\left(x\right)\right| \left(K_m\right)^*\cdot\tau^z\sigma^z\cdot U_m^\dagger\cdot U_r\left|\Psi_\delta\left(x\right)\right\rangle \\ &= i\left\langle v_{\tilde{b}_m}^-\right|\tau^z\left|v_{\tilde{b}_m}^+\right\rangle\sum_{s,s'}\beta_s^*\gamma_{s'}e^{\left(-i\Lambda_m^{-,s}\right)^*L}\left\langle v_{\tilde{\mu}_m}^s\right|\sigma^z\left|v_{\tilde{\mu}_m}^{s'}\right\rangle \\ &= i\frac{\sin\tilde{b}_m}{\sin\tilde{\mu}_m}\,e^{-\sqrt{\Delta_m^2-b_m^2}L}\begin{pmatrix} -e^{\sqrt{B_m^2-\mu_m^2}L}\sin\frac{\theta_l+\tilde{\mu}_m+\tilde{\mu}_l}{2}\sin\frac{\theta_r-\tilde{\mu}_m-\tilde{\mu}_r}{2} \\ +e^{-\sqrt{B_m^2-\mu_m^2}L}\sin\frac{\theta_l-\tilde{\mu}_m+\tilde{\mu}_l}{2}\sin\frac{\theta_r+\tilde{\mu}_m-\tilde{\mu}_r}{2}\end{pmatrix}. \end{aligned} \tag{B43}$$

By taking $\mu_{l,m,r}=0$ (i.e., $\tilde{\mu}_{l,m,r}=\pi/2$), $b_{l,m,r}=0$ (i.e., $\tilde{b}_{l,m,r}=\pi/2$), we restore the previously obtained familiar expressions

$$\langle L|\,\Delta V_L\,|R\rangle_{00}\propto e^{-\Delta_m L}\left(e^{B_m L}\cos\frac{\theta_l}{2}\cos\frac{\theta_r}{2}+e^{-B_m L}\sin\frac{\theta_l}{2}\sin\frac{\theta_r}{2}\right). \tag{B44}$$

6. Majorana Coupling Energy

The energy from perturbative calculation is

$$\begin{aligned} E_{\text{Maj}} &\approx \frac{\langle L|\,\Delta V_L\,|R\rangle}{\sqrt{\langle L|L\rangle\langle R|R\rangle}} \\ &= \frac{1}{\sqrt{M_l\left[\phi_l\right]M_r\left[\phi_r\right]}}\frac{\sin\tilde{b}_m}{\sin\tilde{\mu}_m}e^{-\sqrt{\Delta_m^2-b_m^2}L}\begin{pmatrix} -e^{\sqrt{B_m^2-\mu_m^2}L}\sin\frac{\theta_l+\tilde{\mu}_m+\tilde{\mu}_l}{2}\sin\frac{\theta_r-\tilde{\mu}_m-\tilde{\mu}_r}{2} \\ +e^{-\sqrt{B_m^2-\mu_m^2}L}\sin\frac{\theta_l-\tilde{\mu}_m+\tilde{\mu}_l}{2}\sin\frac{\theta_r+\tilde{\mu}_m-\tilde{\mu}_r}{2}\end{pmatrix}. \end{aligned} \tag{B45}$$

We compare the perturbative calculation with the numerical results. As illustrated in Fig. 2b, we choose the parameters $\mu_{l/m/r}=0$, $b_{l/m/r}=1/2$, $\Delta_m=2.5$, $\Delta_{l/r}=1$, $B_{l/r}=2$, $B_m=1$. For this set of parameters along with $\phi_l=\pi/2$, $\phi_r=\pi$, E is most sensitive to the deviation in ϕ, which gives the max charge current $I_Q\propto\frac{\partial E}{\partial\phi}$.

Appendix C: Analytic Continuation for $\Delta^2<b^2$ or $B^2<\mu^2$

Finally, we extend the applicability of Majorana coupling results to a wider range of parameters by analytic continuation. Note that the above derivation assumes

that both conditions of $\Delta^2 > b^2$ and $B^2 > \mu^2$ are fulfilled over the Δ-B-Δ junction. However, we may further extend the choice of parameters to $\Delta^2 > b^2$ or $B^2 > \mu^2$, so that we may include the possibility of the gapped Δ-phase with $B^2 < \mu^2$ and the gapped B-phase with $\Delta^2 < b^2$. It turns out that Eq. (B45) and its analytic continuation give the correct prediction of the Majorana coupling energy. In this section, we will justify that for $\Delta^2 < b^2$ (or $B^2 < \mu^2$), the coupling energy is consistent with the analytic continuation of Eq. (B45). We basically follow the same procedure as detailed in the previous section, with the following minor modifications to the calculation from Sec. B 3,B 4,B 5.

1. First, we need to generalize $\tilde{b}$ (or $\tilde{\mu}$) from real numbers to complex numbers when consider $\Delta^2 < b^2$ (or $B^2 < \mu^2$):

$$\tilde{b} = \cos^{-1}\frac{b}{\Delta} \equiv -i\cosh^{-1}\frac{b}{\Delta} \tag{C1}$$

or

$$\tilde{\mu} = \cos^{-1}\frac{\mu}{B} \equiv -i\cosh^{-1}\frac{\mu}{B}.$$

2. Correspondingly, the eigensystem of K is

$$K\cdot\left(v_{\tilde{b}}^{s_1}\otimes v_{\tilde{\mu}}^{s_2}\right) = \Lambda^{s_1,s_2}\left(v_{\tilde{b}}^{s_1}\otimes v_{\tilde{\mu}}^{s_2}\right),$$

with sub-eigenvectors

$$v_\xi^s = \frac{1}{\sqrt{2}}\left(-ie^{is\xi/2}, e^{-is\xi/2}\right)^T = v_{s\xi}^+,$$

eigenvalues

$$\Lambda^{s_1,s_2} = \Delta\ \lambda_{\tilde{b}}^{s_1} + B\ \lambda_{\tilde{\mu}}^{s_2},$$

where

$$\lambda_\xi^s = \lambda_{s\xi}^+ = i\sin s\xi = \sinh si\xi \tag{C2}$$

for $s = \pm 1$.

3. For imaginary ξ, the inner product

$$\left(v_\xi^s\right)^T\cdot v_\xi^{s'} = -i\sin s\xi\ \delta_{s,s'} = \begin{pmatrix} -\sinh i\xi & 0 \\ 0 & \sinh i\xi \end{pmatrix} \tag{C3}$$

is consistent with the analytic continuation of Eq.(B19), where $\bar{s} :\equiv -s$ for $s = \pm 1$. Hence, the coefficients $\{\alpha_s, \beta_s, \gamma_s, \delta_s\}$ can be obtained by analytic continuation from Eqs.(B31,B32,B36,B37). For example, $\alpha_s = \sinh^{-1} is\tilde{b}_l = \sinh\frac{is\tilde{b}_l - \left(i\phi_l + i\tilde{b}_m\right)}{2}$.

4. For imaginary ξ, the inner products

$$\left(v_\xi^s\right)^\dagger\cdot\sigma^z\cdot v_\xi^{s'} = i\sin s\xi\ \delta_{s,s'} = \begin{pmatrix} \sinh i\xi & 0 \\ 0 & \sinh i\xi \end{pmatrix} \tag{C4}$$

$$\left(v_\xi^s\right)^\dagger\cdot v_\xi^{s'} = \cosh i\xi\ \delta_{s,s'} + \delta_{\bar{s},s'} = \begin{pmatrix} \cosh i\xi & 1 \\ 1 & \cosh i\xi \end{pmatrix}, \tag{C5}$$

however, do not follow the analytic continuation of Eqs.(B20,B21). This is because the hermitian conjugate does not necessarily follow analytic continuation:

$$\left(v_\xi^s\right)^\dagger = \begin{cases} -v_\xi^s\cdot\sigma^z & \text{for } \xi \text{ imaginary} \\ i\ v_\xi^s\cdot\sigma^x & \text{for } \xi \text{ real} \end{cases}. \tag{C6}$$

5. We need to keep track of different forms of $\left(v_\xi^s\right)^\dagger$ when computing $\langle L|L\rangle$ and $\langle L|\,\Delta V_L\,|R\rangle$ associated with Sec. B 4 and Sec. B 5. After some careful calculation, we can verify that for $\Delta^2 < b^2$ or $B^2 < \mu^2$, the expressions for $\langle L|L\rangle$ and $\langle L|\,\Delta V_L\,|R\rangle$ are still consistent with the analytic continuations of Eqs.(B38,B43).

Therefore, we have justified that the majorana coupling energy can be obtained from the analytic continuation of Eq.(B45) for $\Delta^2 < b^2$ or $B^2 < \mu^2$.

In summary, we have analyzed the 1D system described by Hamiltonian $H(\mu, \Delta, \phi; b, B, \theta)$ with three phases**:** Δ-phase $\left(\Delta^2 - b^2 > \max\left[B^2 - \mu^2, 0\right]\right)$, B-phase $\left(B^2 - \mu^2 > \max\left[\Delta^2 - b^2, 0\right]\right)$, and gapless phase ($B^2 \le \mu^2$ and $\Delta^2 \le b^2$). For B-Δ-B junction hosting two Majoranas with separation L, the Majorana coupling energy can be expressed as Eqs.(B45,B38) is:

$$\frac{E_{\text{Maj}}}{E_0\left[\delta\phi_{l,r}\right]} \approx e^{-\lambda_{m,1}L}\sin\frac{\delta\theta_l - \tilde{\mu}_m + \tilde{\mu}_l}{2}\sin\frac{\delta\theta_r + \tilde{\mu}_m - \tilde{\mu}_r}{2} - e^{-\lambda_{m,2}L}\sin\frac{\delta\theta_l + \tilde{\mu}_m + \tilde{\mu}_l}{2}\sin\frac{\delta\theta_r - \tilde{\mu}_m - \tilde{\mu}_r}{2}, \tag{C7}$$

with $\tilde{\mu}_{l/m/r} \equiv \cos^{-1}\frac{\mu_{l/m/r}}{B_{l/m/r}}$, $\tilde{b}_{l/m/r} \equiv \cos^{-1}\frac{b_{l/m/r}}{\Delta_{l/m/r}}$. Here we introduce $\delta\phi_{\ell,r} \equiv \phi_{\ell,r} - \phi_m$, $\delta\theta_{\ell,r} \equiv \theta_{\ell,r} - \theta_m$ to restore the dependence of E_{Maj} on ϕ_m and θ_m. The characteristic energy is

$$E_0\left[\delta\phi_{l,r}\right] = \frac{\sin\tilde{b}_m}{\sin\tilde{\mu}_m}\frac{1}{\sqrt{M_l\left[\delta\phi_l\right]M_r\left[\delta\phi_r\right]}}, \tag{C8}$$

where the normalization of Majorana wavefunction is

$$M_s\left[\delta\phi_s\right] \approx \frac{\left(\Delta_m^2+\mu_m^2-b_m^2\right)}{2\sqrt{\Delta_m^2-b_m^2}\left(\Delta_m^2+\mu_m^2-B_m^2-b_m^2\right)}+\frac{\left(B_s^2+b_s^2-\mu_s^2\right)+\Delta_s\left[\sqrt{B_s^2-\mu_s^2}\sin\left(\tilde{b}_m\pm\delta\phi_s\right)-b_s\cos\left(\tilde{b}_m\pm\delta\phi_s\right)\right]}{2\sqrt{B_s^2-\mu_s^2}\left(B_s^2+b_s^2-\Delta_s^2-\mu_s^2\right)}, \tag{C9}$$

with the choice of sign $\pm$ depending on $s=l$ or r. Note that M_s exhibits the standard 2π periodicity in $\delta\phi_s$, so that the more exotic 4π periodicity follows exclusively from the trigonometric functions in Eq. (C7).

[1] L. Fu and C. L. Kane, Phys. Rev. B **79**, 161408 (2009).
[2] R. M. Lutchyn, J. D. Sau, and S. Das Sarma, Phys. Rev. Lett. **105**, 077001 (2010).
[3] Y. Oreg, G. Refael, and F. von Oppen, Phys. Rev. Lett. **105**, 177002 (2010).
[4] L. Jiang, D. Pekker, J. Alicea, G. Refael, Y. Oreg, and F. von Oppen, Phys. Rev. Lett. **107**, 236401 (2011).
[5] C. Beenakker, arXiv: 1112.1950.
[6] Y. Asano and Y. Tanaka, arXiv: 1204.4226.
[7] J. Alicea, Rep. Prog. Phys. **75**, 076501 (2012).
[8] K. Sengupta, I. Zutic, H.-J. Kwon, V. M. Yakovenko, and S. Das Sarma, Phys. Rev. B **63**, 144531 (2001).
[9] C. J. Bolech and E. Demler, Phys. Rev. Lett. **98**, 237002 (2007).
[10] K. T. Law, P. A. Lee, and T. K. Ng, Phys. Rev. Lett. **103**, 237001 (2009).
[11] K. Flensberg, Phys. Rev. B **82**, 180516 (2010).
[12] L. Fidkowski, J. Alicea, N. Lindner, R. Lutchyn, and M. Fisher, arXiv: 1203.4818.
[13] V. Mourik, K. Zuo, S. M. Frolov, S. R. Plissard, E. P. A. M. Bakkers, and L. P. Kouwenhoven, Science **336**, 1003 (2012).
[14] M. T. Deng, C. L. Yu, G. Y. Huang, M. Larsson, P. Caroff, and H. Q. Xu, arXiv: 1204.4130.
[15] A. Das, Y. Ronen, Y. Most, Y. Oreg, M. Heiblum, and H. Shtrikman, arXiv: 1205.7073.
[16] N. Read and D. Green, Phys. Rev. B **61**, 10267 (2000).
[17] D. A. Ivanov, Phys. Rev. Lett. **86**, 268 (2001).
[18] J. Alicea, Y. Oreg, G. Refael, F. von Oppen, and M. P. A. Fisher, Nat. Phys. **7**, 412 (2011).
[19] L. Fu, Phys. Rev. Lett. **104**, 056402 (2010).
[20] A. Kitaev, Physics-Uspekhi **44**, 131 (2001).
[21] F. S. Nogueira and K. H. Bennemann, EPL (Europhysics Letters) **67**, 620 (2004).
[22] Y. Asano, Phys. Rev. B **74**, 220501 (2006).
[23] P. M. R. Brydon, Phys. Rev. B **80**, 224520 (2009).
[24] P. M. R. Brydon, Y. Asano, and C. Timm, Phys. Rev. B **83**, 180504 (2011).
[25] T. Birol and P. W. Brouwer, Phys. Rev. B **80**, 014434 (2009).
[26] *In preparation.*
[27] D. M. Badiane, M. Houzet, and J. S. Meyer, Phys. Rev. Lett. **107**, 177002 (2011).
[28] P. San-Jose, E. Prada, and R. Aguado, arXiv: 1112.5983.
[29] J. M. Kikkawa and D. D. Awschalom, Science **287**, 473 (2000).
[30] C. P. Slichter, *Principles of magnetic resonance*, Springer series in solid-state sciences ; 1 (Springer-Verlag, Berlin ; New York, 1990), 3rd ed.
[31] A. Willig, B. Sapoval, K. Leibler, and C. Verie, Journal of Physics C: Solid State Physics **9**, 1981 (1976).
[32] A. Cehovin, C. M. Canali, and A. H. MacDonald, Phys. Rev. B **68**, 014423 (2003).
[33] A. Brataas, A. D. Kent, and H. Ohno, Nat Mater **11**, 372 (2012).
[34] A. Romito, J. Alicea, G. Refael, and F. von Oppen, Phys. Rev. B **85**, 020502(R) (2012).
[35] Q. Meng, V. Shivamoggi, T. L. Hughes, M. J. Gilbert, and S. Vishveshwara, arXiv: 1206.1295.
[36] P. Kotetes, G. Schon, and A. Shnirman, arXiv: 1207.2691.
[37] J. Nilsson, A. R. Akhmerov, and C. W. J. Beenakker, Phys. Rev. Lett. **101**, 120403 (2008).
[38] Technically, interpreting Eq. (1) as a spin current is valid when one employs topological insulators with globally conserved S^z.
[39] In fact, a similar duality can be constructed for a tight-binding description of a spin-orbit coupled quantum wire.
[40] In contrast to the ϕ dependent 4π periodic Josephson effect, it requires *opposite* domain sequence in a TI edge (Δ-B-Δ) and in semiconductor wires (T-NT-T) [4]. This arises since the paired large-momentum Fermi points form a p-wave superconductor. If the $p=0$ crossing forms another p-wave superconductor, together the two form a topologically trivial phase.